Nanoscale Research Letters
a SpringerOpen Journal

NANO EXPRESS Open Access

The influence of anatase-rutile mixed phase and ZnO blocking layer on dye-sensitized solar cells based on TiO_2nanofiberphotoanodes

Jianning Ding[1,2*], Yan Li[1], Hongwei Hu[1], Li Bai[1], Shuai Zhang[1,2] and Ningyi Yuan[1,2*]

Abstract

High performance is expected in dye-sensitized solar cells (DSSCs) that utilize one-dimensional (1-D) TiO_2 nanostructures owing to the effective electron transport. However, due to the low dye adsorption, mainly because of their smooth surfaces, 1-D TiO_2 DSSCs show relatively lower efficiencies than nanoparticle-based ones. Herein, we demonstrate a very simple approach using thick TiO_2 electrospun nanofiber films as photoanodes to obtain high conversion efficiency. To improve the performance of the DSCCs, anatase-rutile mixed-phase TiO_2 nanofibers are achieved by increasing sintering temperature above 500°C, and very thin ZnO films are deposited by atomic layer deposition (ALD) method as blocking layers. With approximately 40-μm-thick mixed-phase (approximately 15.6 wt.% rutile) TiO_2 nanofiber as photoanode and 15-nm-thick compact ZnO film as a blocking layer in DSSC, the photoelectric conversion efficiency and short-circuit current are measured as 8.01% and 17.3 mA cm^{-2}, respectively. Intensity-modulated photocurrent spectroscopy and intensity-modulated photovoltage spectroscopy measurements reveal that extremely large electron diffusion length is the key point to support the usage of thick TiO_2 nanofibers as photoanodes with very thin ZnO blocking layers to obtain high photocurrents and high conversion efficiencies.

Keywords: Dye-sensitized solar cell, Titanium dioxide nanofiber photoanode, Anatase-rutile mixed phase, Zinc oxide blocking layer, Atomic layer deposition method

Background

Due to their cost-effectiveness, ease of manufacturing, and suitability for large-area production, dye-sensitized solar cells (DSSCs) have attracted much attention. Typically, the photoanode of a DSSC is made of a TiO_2 nanoparticle film (10-μm thickness) adsorbed with a monolayer Ru-based complex dye. Although the certified energy conversion efficiency of DSSCs has exceeded 12% [1], electrons generated from photoexcited dyes injected into the conduction band of TiO_2 will pass through the grain boundaries and interparticle connections, which are strongly influenced by the surface trapping/detrapping effect, leading to slow electron transport [2]. One-dimensional (1-D) nanostructures have superior electron transport characteristics compared to nanoparticle-based systems [3,4]. Several methods have been established for the preparation of 1-D structured TiO_2, including nanowires [5,6], nanotubes [7-10] and nanofibers. Among the methods for preparing 1-D TiO_2 nanostructures, electrospinning provides a versatile, simple, and continuous process [11-13]. However, even though extremely fast electron transport is available in the 1-D nanostructures, these 1-D TiO_2-based DSSCs usually show relatively lower efficiencies than nanoparticle-based ones, mainly because of low dye adsorption. To solve this problem of TiO_2 electrospun nanofiber DSSCs, some attempts have been done, such as applying mechanical pressure to break the outer sheaths of nanofibers to increase surface area [14,15], calcination of nanofibers with a hot pressing pre-treatment to obtain multi-core cable-like nanofibers [16]. However, these methods destroy continuous 1-D nanostructures. In view of the excellent electron transport characteristic, which will result in a large diffusion length, it is feasible to increase the thickness of 1-D nanostructure photoanodes to improve dye adsorption

* Correspondence: dingjn@cczu.edu.cn; nyyuan@cczu.edu.cn
[1]Center for Low-dimensional Materials, Micro-nano Devices and System, Changzhou University, Changzhou 213164, China
[2]Jiangsu Key Laboratory for Solar Cell Materials and Technology, Changzhou 213164, China

and, consequently, to enhance the conversion efficiency of cells. Unfortunately, the lengths of TiO_2 nanowires or nanorods are usually several micrometers [5,6], and it is a very difficult or time-consuming mission to enlarge their length, so the conversion efficiency is limited. Long TiO_2 nanotube can be formed by anodization of titanium foils [17]. However, backside-illumination mode of anodized TiO_2 nanotube-based solar cells is an obstacle for realizing a high efficiency since the redox electrolyte containing the iodine species has an absorption in near UV spectrum and platinum-coated fluorine-doped SnO_2 (FTO) partially and inevitably reflects light [17,18]. On the contrary, it is very easy within a short period of process to enlarge the thickness of TiO_2 electrospun nanofiber photoanode on FTO substrates for front illumination.

On the other hand, superior performance of anatase-rutile mixed-phase TiO_2 nanoparticle DSSCs with a small amount of rutile to pure phase ones was claimed [19,20]. Different from nanoparticles, it is relatively difficult for nanowires or nanotubes to control their crystalline phase, so there are little researches on anatase-rutile mixed-phase 1-D TiO_2 DSSCs. Besides, it has been proven effective to block electron recombination by introduction of a compact layer, such as TiO_2 [21-25], Nb_2O_5 [26], and ZnO [27,28] between the FTO and porous TiO_2. Nb_2O_5 is an expensive material for compact film. For ZnO, not only electron transmission is faster than that in TiO_2 but also its conduction band edge is a little more negative than that of TiO_2, which will introduce an energy barrier at the interface of FTO/TiO_2. The energy barrier will be favorable to suppress the back electron transfer from FTO to electrolytes. However, the thickness of the reported ZnO blocking layers deposited by sputtering methods [27,28] was around 150 nm to get the highest conversion efficiency. Thick blocking layers will reduce transmittance of FTO substrates and consequently decrease the absorption of visible light. Meanwhile, it probably retards the transport of injected electrons from TiO_2 conduction band to FTO, resulting in a low photocurrent [28]. Atomic layer deposition (ALD) technique can produce continuous, angstrom-level-controlled, and defect-free films, which is very suitable to deposit ultrathin compact film.

In this paper, to make the best of excellent electron transport characteristic of 1-D nanostructures, thick TiO_2 nanofiber films were used as photoanodes to fabricate DSSCs. Meanwhile, anatase-rutile mixed-phase TiO_2 nanofibers obtained by increasing sintering temperature and very thin ZnO compact layers deposited by ALD method were first adopted in the TiO_2 nanofiber DSSC fabrication to further improve photocurrent and conversion efficiency. Combining the above two steps, a short-circuit current density of 17.3 mA cm^{-2} and a conversion efficiency of 8.01% were achieved for the DSSC using approximately 40-μm-thick TiO_2 nanofiber film as photoanode. Intensity-modulated photocurrent spectroscopy (IMPS) and intensity-modulated photovoltage spectroscopy (IMVS) were used to investigate the dynamic response of charge transfer and recombination in TiO_2 nanofiber DSSCs.

Methods

TiO_2 nanofiber synthesis

The polyvinylpyrrolidone (PVP)-TiO_2 nanofibers were fabricated using electrospinning technique. Typically, the precursor solution for electrospinning was made from 0.45 g of PVP (with a molecular weight of 1,300,000; Sigma-Aldrich Corporation, St. Louis, MO, USA), 7 ml of ethanol, 2 ml of acetic acid, and 1 g of titanium (IV) isopropoxide (Sigma-Aldrich). In a typical electrospinning procedure, the precursor solution was loaded into a syringe equipped with a 24 gauge silver-coated needle. The needle was connected to a high-voltage power supply. The electric voltage of 16 kV was applied between the metal orifice and the Al collector at a distance of 10 cm. The spinning rate was controlled by the syringe pump at 60 μl min^{-1}. After the electrospinning procedure, the PVP-TiO_2 fiber composite films were then heated at a rate of 4°C min^{-1} up to 500°C, 550°C, 600°C, and 700°C, respectively, and then sintered at this temperature for 2 h to obtain pure TiO_2-based nanofibers.

Preparation of ultrathin ZnO blocking layers by ALD method

ZnO layers were deposited on FTO-coated glass substrates (25 Ω/sq) by ALD method. FTO glass plates were first cleaned in a detergent solution using an ultrasonic bath for 15 min and were then rinsed with water and ethanol. Diethylzinc (DEZ; $Zn(C_2H_5)_2$) and deionized water were used as precursors for ZnO deposition on the cleaned FTO plates. Pure N_2 gas (99.999%) was used to carry and purge gas. The reaction was carried out as follows:

$$Zn(C_2H_5)_2 + H_2O \rightarrow Zn\,O + 2C_2H_6 \quad (1)$$

Before deposition, the reaction chamber was pumped down from 1 to 2 Torr. The operating environment of ZnO deposition was maintained at 3 Torr and 200°C. Each deposition cycle consisted of four steps, which included DEZ reactant, N_2 purge, H_2O reactant, and N_2 purge. The typical pulse time for introducing DEZ and H_2O precursors was 0.5 s, and the purge time of N_2 was 10 s. The deposition rate of ZnO film at the above conditions approached 0.182 nm/cycle. Thus, the deposition

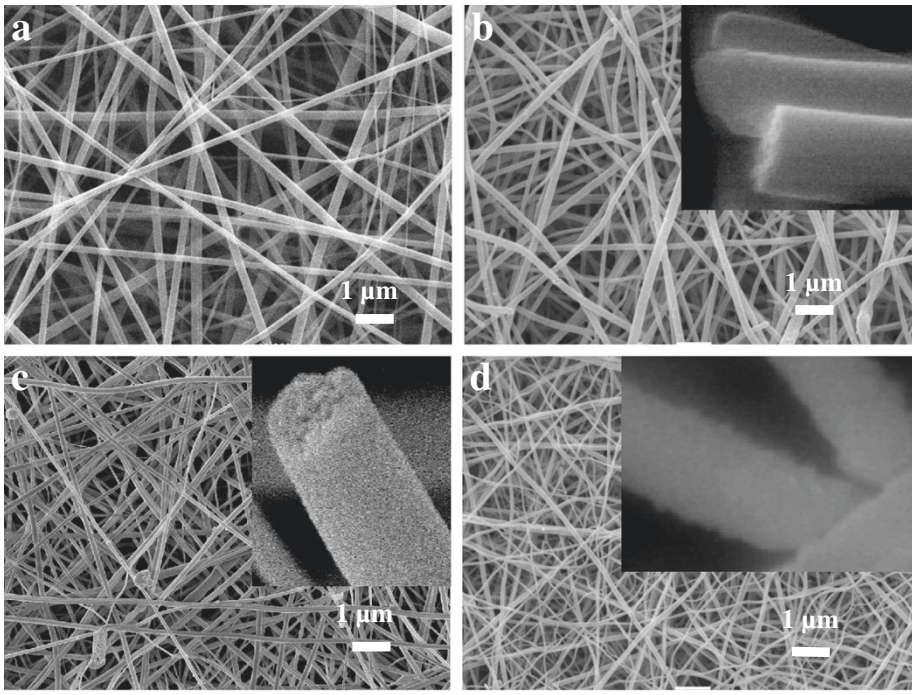

Figure 1 SEM images of electrospun nanofibers. As-spun TiO_2-PVP nanofibers (**a**), TiO_2 nanofibers after calcination at 500°C (**b**), 550°C (**c**), and 600°C (**d**). The insets in b, c, and d are high-magnification photos of single nanofibers.

cycles of 22, 55, 83, and 110 were chosen to produce ZnO layers with thicknesses of 4, 10, 15, and 20 nm.

Solar cell fabrication and characterization

First, the substrates were coated with TiO_2 nanofiber films using a mixed solution (20 ml ethanol and 2 ml titanium (IV) isopropoxide) for enhancing the adhesion between TiO_2 films and substrates, and were subsequently sintered at 500°C for 30 min to ensure good electrical contact between the TiO_2 nanofiber films and the FTO substrates. Then, the TiO_2 electrodes were immersed into the N-719 dye solution (0.5 mM in ethanol) and were held at room temperature for 24 h. The dye-treated TiO_2 electrodes were rinsed with ethanol and dried under nitrogen flow. For the counter electrodes, the FTO plates were drilled and coated with a drop of 10 mM H_2PtC_{l6} (99.99%, Sigma-Aldrich) solution and were then heated at 400°C for 20 min. The liquid electrolyte was prepared by dissolving 0.6 M of 1-butyl-3-methylimidazolium iodide, 0.03 M of iodine, 0.1 M of guanidinium thiocyanate, and 0.5 M of 4-*tert*-butylpyridine in acetonitrile/valeronitrile (85:15 *v*/*v*). Finally, dye-coated TiO_2 films and Pt counter electrodes were assembled into sealed sandwich-type cells by heating with hot-melt films used as spacers. The typical active area of the cell was 0.25 cm^2.

The crystallographic structure of the nanofiber was analyzed by X-ray diffraction (XRD) (D/MAX Ultima III, Rigaku Corporation, Tokyo, Japan) using Cu Kα radiation. The morphology was determined by scanning electron microscopy (SEM). Specific surface areas of the nanofibers in powder form were measured with a Quantachrome Autosorb-3b static volumetric instrument (Quantachrome Instruments, Boynton Beach, FL, USA). UV-visible (UV–vis) spectra were carried out on a Hitachi U-3010 spectrophotometer (Hitachi, Ltd., Chiyoda, Tokyo, Japan).

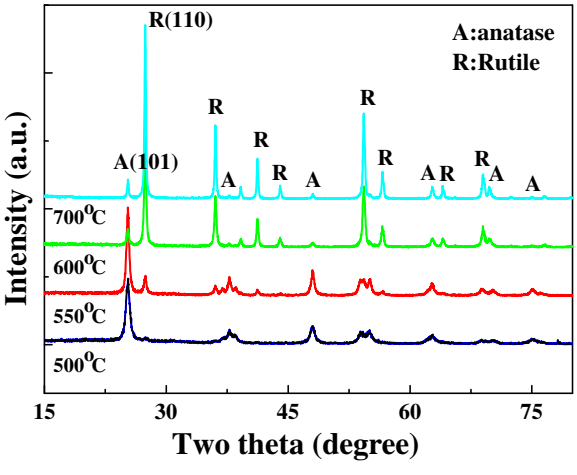

Figure 2 XRD patterns of TiO_2 nanofibers sintered at 500°C, 550°C, 600°C, and 700°C. The diffractions of anatase and rutile phase are labeled in the figure as 'A' and 'R', respectively.

The thicknesses of the films were obtained using an α-Step 500 surface-profile measurement system (KLA-Tencor Corporation, Milpitas, CA, USA). Photovoltaic characteristics were measured using a Keithley 2400 source meter (Keithley Instruments Inc., Cleveland, OH, USA). A solar simulator (500-W Xe lamp) was employed as the light source, and the light intensity was adjusted with a Si reference solar cell for approximating AM 1.5 global radiation. IMPS and IMVS spectra were measured on a controlled intensity-modulated photospectroscopy (Zahner Co., Kansas City, MO, USA) in ambient conditions under illumination through the FTO glass side, using a blue light-emitting diode as the light source (BLL01, λ_{max} = 470 nm, spectral half-width = 25 nm; Zahner Co.) driven by a frequency response analyzer, and the light intensity (incident photon flux) of the DC component was controlled at 2.5×10^{16} cm^{-2} s^{-1}. During the IMVS and IMPS measurements, the cell was illuminated with sinusoidally modulated light having a small AC component (10% or less of the DC component).

Results and discussion

Characterization of TiO_2 nanofibers

The surface morphologies of as-spun TiO_2-PVP composite and sintered TiO_2 nanofibers were characterized by SEM as shown in Figure 1. It is found that the network structure of the former is maintained after calcinations in air to remove PVP, forming a porous TiO_2 membrane. The higher sintering temperature, the thinner is TiO_2 fiber. The average fiber diameter of the composite nanofibers is 290 ± 90 nm which decreases to 210 ± 60 nm, 180 ± 70 nm, and 140 ± 80 nm after sintering at 500°C, 550°C, and 600°C, respectively. It is known that crystalline grains of anatase TiO_2 are spherical, while rutile ones are of rod structure. With the increase of the sintering temperature, some anatase TiO_2 grains will transform to rutile ones, which may result in the thinning of the fibers. Moreover, transformation of anatase TiO_2 grains to rutile ones will introduce stress in the fibers, which will cause the fibers to become brittle and even fracture. The insets in Figure 1b, c, d are high-magnification photos of nanofibers, which indicate that the surfaces of TiO_2 nanofibers sintered at 500°C and 550°C are rather smooth, while become a little rough when sintering temperature increases to 600°C. Figure 2 shows the XRD patterns of TiO_2 nanofibers. All the peaks of the TiO_2 nanofibers sintered at 500°C are indexed for anatase TiO_2 with dominant (101) peaks. The mean grain size determined from the XRD pattern using the Scherrer formula is around 16 nm. The nanofibers sintered at 550°C, 600°C, and 700°C are observed to contain both anatase and rutile phases. The phase composition can be determined from XRD results according to the following equation [29]:

$$W_R = A_R/(0.884 \times A_A + A_R) \quad (2)$$

where W_R, A_A, and A_R represent rutile weight percentage, integrated intensity of anatase (101) peak, and rutile (110) peak, respectively [29]. The calculated rutile contents in the above three mixed-phase nanofiber samples are approximately 15.6, 87.8, and 90.5 wt.%, and the mean grain sizes are 22, 30, and 42 nm, respectively. The XRD results indicate that with the increase of sintering temperature, the grain size is gradually increased; however, rutile content is sharply increased in the temperature range of 550°C to 600°C.

Characterization of ultrathin ZnO layers deposited by ALD method

To detect the crystallographic structure and thickness of ZnO layers, except FTO substrates, glass substrates were also used to deposit ZnO layers. XRD patterns for ZnO layers deposited on glass substrate are shown in Figure 3a. A 4-nm-thick ZnO layer does not show any diffraction peak, whereas peaks corresponding to hexagonal phase ZnO are observed for the thickness of 10 or 20 nm, which indicates that the deposited ZnO layers by ALD method are polycrystalline. Figure 3b shows the UV–vis transmission spectra for the FTO substrates without ZnO layers and with ZnO layers of different thicknesses. The absorbance edges for the bare FTO and ZnO are around 315 and 380 nm, respectively, from which the bandgap of ZnO is calculated to be 3.2 to 3.3 eV. In the visible range, the transmittance of the FTO covered with ZnO decreases slightly with the increase of ZnO film thickness. For instance, it decreases to approximately 95% of the transmittance of the bare FTO for 20-nm-thick ZnO. Therefore, the presence of ZnO layer with the thickness less than 20 nm will not obviously influence the harvest of light. The inset in Figure 3b is the SEM photo of FTO substrate covered with 15-nm-thick ZnO film, which shows that the ZnO film deposited by ALD method keeps the surface morphology of FTO substrate very well.

Performance of DSSCs

The influence of sintering temperature of TiO_2 nanofiber photoanodes on the performance of TiO_2 nanofiber cells

Cells I to III are TiO_2 nanofiber cells (sintered at 500°C, 550°C, and 600°C) on the bare FTO substrates. Based on the above photocurrent-voltage(*J-V*) measurement results, a thickness of approximately 40 μm was set to fabricate cells I to III. Figure 4 illustrates the *J-V*

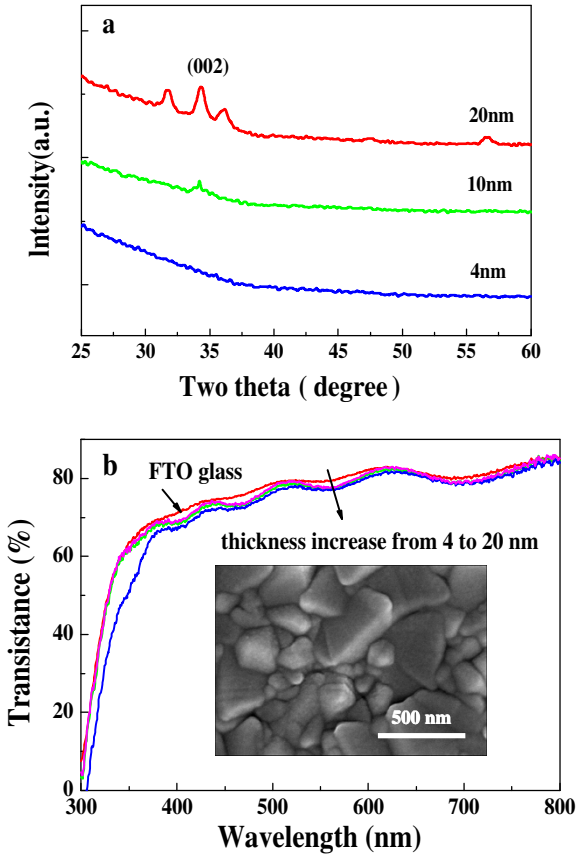

Figure 3 XRD patterns. ZnO layers deposited on glass substrate (**a**) and UV–vis transmission spectra for the FTO substrate without and with ZnO layers (**b**). The inset in b is the SEM photo of FTO substrate covered with 15-nm-thick ZnO film.

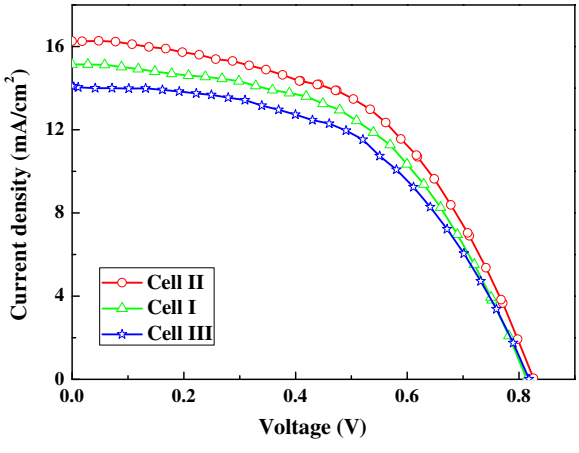

Figure 4 Photocurrent-voltage characteristics of cells I to III under AM 1.5 irradiation of 100 mW cm^{-2}. Based on TiO_2 nanofibers sintered at 500°C, 550°C, and 600°C.

characteristics of TiO_2 nanofiber cells under AM 1.5 irradiation of 100 mW cm^{-2}. The photovoltaic properties such as short-circuit current density (J_{sc}), open-circuit voltage (V_{oc}), fill factor (FF), and photoelectric conversion efficiency (PCE) of the cells are listed in Table 1. Cell I has a J_{sc} of 15.1 mA cm^{-2}, PCE of 6.39%, V_{oc} of 0.814 V, and fill factor (FF) of 0.52. When sintering temperature increased from 500°C to 550°C, cell II gave an improvement of J_{sc} and V_{oc} about 1.2 mA cm^{-2} and 11 mV, respectively, resulting in an efficiency of 7.12%. However, the further increase of sintering temperature decreased J_{sc}, V_{oc}, and PCE of cell III to 14.1 mA cm^{-2}, 0.818 V, and 6.11%, respectively. According to the XRD data, rutile contents of TiO_2 nanofibers are approximately 0, 15.6, and 87.8 wt.% in cells I, II, and III, respectively. The *J-V* measurement results demonstrate that the anatase-rutile mixed-phase TiO_2 nanofiber with a low rutile content is good for enhancing efficiencies of the DSSCs, whereas a high rutile content is detrimental to the efficiencies, which is similar to the reported DSSCs based on mixed-phase TiO_2 nanoparticles [19,20].

In this study, specific surface areas were measured to be 28.5, 31.7, and 34.2 m^2 g^{-1} for TiO_2 nanofibers sintered at 500°C, 550°C, and 600°C, respectively, which indicate that thinner rough nanofibers sintered at a higher temperature is favorable to increase the specific surface areas. UV–vis absorption spectra (Figure 5) of the sensitized TiO_2 nanofiber film show that the absorption edges are successfully extended to the visible region for all the three samples. In contrast with pure anatase phase (sintered at 500°C), mixed-phase TiO_2 nanofibers (sintered at 550°C and 600°C) after N719 sensitization absorb a greater portion of the visible light, which should be the result of joint contribution of large specific surface area and mixed phase. Because anatase phase TiO_2 has the greatest dye absorption ability, while rutile phase TiO_2 possesses excellent light scattering characteristics due to its high refractive index (n = 2.7) [25,26], dye-sensitized anatase-rutile mixed-phase TiO_2 with a proper proportion will have an enhanced light absorption.

The IMPS and IMVS plots of cells I to III display semicircles in the complex plane as shown in Figure 6. The transit time (τ_d) and electron lifetime (τ_n) can be calculated using the equations $\tau_d = 1/(2\pi f_{IMPS,min})$ and $\tau_n = 1/(2\pi f_{IMVS,min})$, respectively, where $f_{IMPS,min}$ and $f_{IMVS,min}$ are the frequencies at the minimum imaginary component in the IMPS and IMVS plots [30]. The estimated electron lifetimes of the three cells follow the trend $\tau_{n\ II} > \tau_{n\ III} > \tau_{n\ I}$, suggesting a reduction in recombination of electrons at the interface between TiO_2 and electrolyte in the presence of rutile phase, while transit times vary in the order $\tau_{d\ II} > \tau_{d\ I} > \tau_{d\ III}$,

Table 1 Photocurrent density-voltage characteristics of TiO_2 nanofiber cells sintered at 500°C, 550°C, and 600°C

Cell	Temperature (°C)	J_{sc} (mA/cm^2)	V_{oc} (V)	FF	η (%)	τ_d (ms)	τ_n (ms)	L_n (μm)
I	500	15.1	0.814	0.52	6.39	3.36	55.3	74.2
II	550	16.3	0.825	0.53	7.12	1.88	107.7	138.3
III	600	14.1	0.818	0.53	6.11	6.47	86.9	67.1

TiO_2 nanofiber cells on the bare FTO substrates, the transit time (τ_d) and electron lifetime (τ_n), and diffusion length (L_n).

indicating that the variation in electron transport rate is dependent on the amount of rutile phase. The competition between collection and recombination of electrons can be expressed in terms of the electron diffusion length. The electron collection efficiency is determined by the effective electron diffusion length, L_n, [31]:

$$L_n = d(\tau_n/2.35\tau_d)^{1/2} \quad (3)$$

where d is the thickness of the photoanode. The calculated L_n/d (as shown in Table 1) of TiO_2 nanofiber cell is large and follows the sequence $L_{n\ II}/d_{II} > L_{n\ I}/d_I > L_{n\ III}/d_{III}$. A remarkable large value of 4.9 is found for cell II. A large electron diffusion length is the key point to support the usage of thick TiO_2nanofibers as photoanodes to obtain high photocurrents and high conversion efficiencies. The largest L_n/d_{II} of cell II with 15.6% rutile content is speculated to be caused by the interaction of rutile and anatase phases which prompts electron transfer from anatase to rutile due to their different conduction band edge and decreased charge recombination rate. However, if the amount of rutile phase is too high in TiO_2 nanofibers, such as 87.8% in cell III, the property of rutile phase will play a leading role in the cell. A large transit time shows a slow electron transport in cell III, which leads to a decrease in electron diffusion length for cell III. From the above analysis, it is concluded that the superior J_{sc} of cell II is a consequence of more efficient electron collection and light harvesting. As far as V_{oc} is concerned, it is known that V_{oc} corresponds to the energy difference between the quasi-Fermi level of the electrons in the TiO_2 under illumination and the redox potential. If the electron recombination is retarded, the electron density in the conduction band of TiO_2 will be increased, which will result in a negative shift in quasi-Fermi level, thereby V_{oc} will be increased [32]. Thus, the higher V_{oc} of cell II is ascribed to the reduced electron recombination rate. For cell III, in spite of the largest absorbance of visible light, a relatively low J_{sc} is produced because of an inefficient electron collection. The comparison of cells I to III highlights the

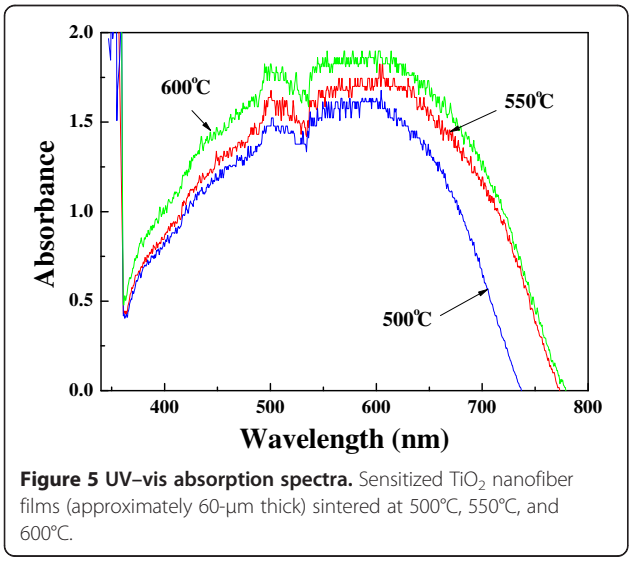

Figure 5 UV–vis absorption spectra. Sensitized TiO_2 nanofiber films (approximately 60-μm thick) sintered at 500°C, 550°C, and 600°C.

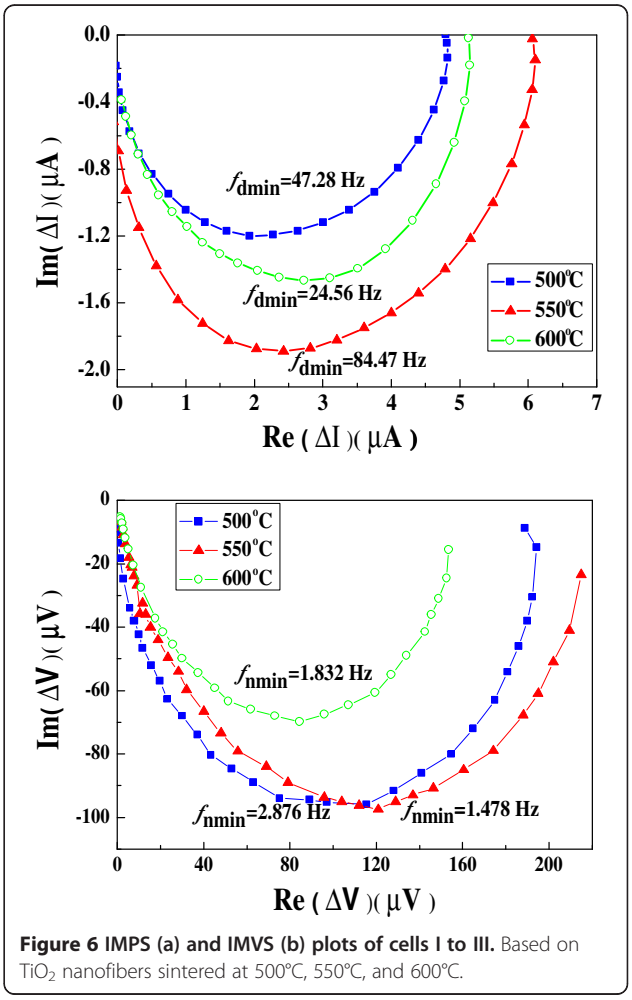

Figure 6 IMPS (a) and IMVS (b) plots of cells I to III. Based on TiO_2 nanofibers sintered at 500°C, 550°C, and 600°C.

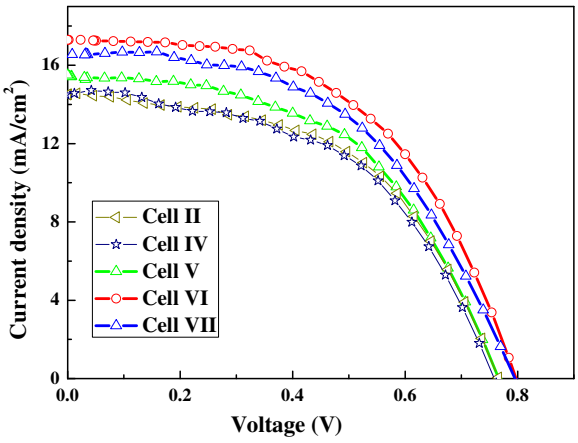

Figure 7 Photocurrent-voltage curves of TiO_2 nanofiber cells (sintered at 550°C and approximately 60-μm thick). With ZnO layer of different thicknesses (4 to 20 nm).

existence of a synergistic effect between the anatase and rutile phases in TiO_2 nanofiber DSSCs, as well as suggests a sintering temperature of approximately 550°C which is optimal for enhancing the performance of nanofiber DSSCs.

The influence of ZnO blocking layer on the performance of TiO_2 nanofiber cells

Based on the above results, cell II was chosen as the reference cell to study the influence of ZnO blocking layer on the performance of TiO_2 nanofiber cells. ZnO layers with thicknesses of 4, 10, 15, and 20 nm were deposited by ALD method on FTO substrates to fabricate cells IV, V, VI, and VII, respectively. *J-V* curves of cells II and IV to VII are shown in Figure 7, and the photovoltaic characteristics of these cells are summarized in Table 2. Compared with cell II, the performances of the cells with the ZnO layer are significantly improved. With the ZnO layer thickness increased from 0 to 15 nm, J_{sc} of the cells is monotonously boosted, but when decreased obviously at 20 nm, it is still larger than that without the ZnO layer. It is noticed that enhancement in V_{oc} and FF is very small. The largest J_{sc} of 17.3 mA cm^{-2} is obtained from cell VI with 15-nm-thick ZnO layer, resulting in the highest PCE of 8.01%, in contrast with 16.3 mA cm^{-2} and 7.12% of reference cell II. This phenomenon indicates that the charge collection of the cells is improved by the blocking function of ZnO layer on interfacial recombination, which is very different from the reported decrease of J_{sc} caused by thick ZnO blocking layers [30].

The schematic view of electron transfer with ZnO layer is shown in Figure 8. The interfacial processes involved in charge transportation in the cell are depicted in Figure 8b. As exciton dissociation occurs, electrons injected into the TiO_2 conduction band will transport to the FTO by diffusion [33]. Because the conduction band edge of ZnO is a little more negative than that of TiO_2, an energy barrier is introduced at the interface of FTO/TiO_2, in which ultrathin ZnO layer can effectively suppress the back electron transfer from FTO to electrolytes or may block injected electron transfer from TiO_2 to FTO. The back reaction was studied using IMVS measurements. The electron lifetime τ_n obtained from IMVS (as shown in Table 2) is 107.7 ms for the cell without ZnO layer but is significantly increased from 119.5 to 354.5 ms with ZnO layer thickness increasing from 4 to 20 nm. The striking increase in the lifetime shows direct evidence that ultrathin ZnO layers prepared by ALD method successfully suppress the charge recombination between electrons emanating from the FTO substrate and I_3^- ions in the electrolyte. The transit times of electrons calculated from IMPS measurements reflect charge transport and back reaction. Although an energy barrier is induced by introduction of ZnO layer between the TiO_2 and FTO, the electron transit time estimated from IMPS measurement is decreased from 1.88 to 1.08 ms for cells with ZnO layer thickness increasing from 0 to 15 nm. However, when the thickness of ZnO layer further increases, the change trend is reverse, and electron transit time for the cell with 20-nm-thick ZnO layer is markedly increased to 4.62 ms. It is put forward that relative to the cell without ZnO blocking layer, the electron transport in the cells with ZnO layers is determined by the two competition roles of the suppression effect of recombination with I_3^- and potential barrier blocking effect. The increased electron lifetime has verified that ultrathin ZnO layer effectively slows the back recombination of electrons at the interface of FTO/electrolyte, so

Table 2 Photocurrent density-voltage characteristics of TiO_2 nanofiber cells

Cell	ZnO thickness (nm)	J_{sc} (mA/cm^2)	V_{oc} (V)	FF	η (%)	τ_d (ms)	τ_n (ms)	L_n (μm)
II	0	14.5	0.825	0.53	6.34	1.88	107.7	138.3
IV	4	15.0	0.828	0.54	6.71	1.43	119.5	166.9
V	10	16.5	0.833	0.54	7.42	1.21	154.3	206.4
VI	15	17.3	0.842	0.55	8.01	1.08	179.7	235.7
VII	20	14.8	0.825	0.53	6.47	4.62	354.5	159.9

TiO_2 nanofiber cells with ZnO layer of different thicknesses, the transit time (τ_d) and electron lifetime (τ_n), and diffusion length (L_n).

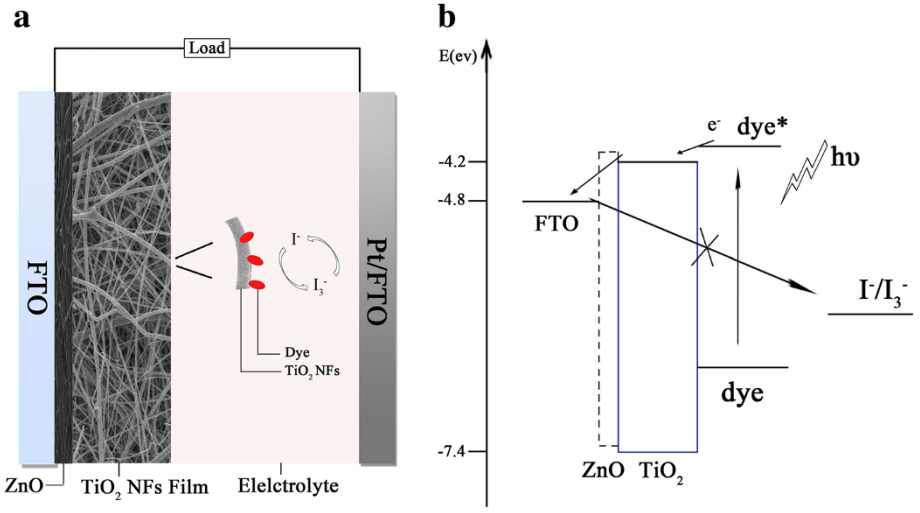

Figure 8 Schematic view of electron transfer with ZnO layer. TiO_2 nanofiber DSSC with an ultrathin ZnO layer (**a**). Illustration of the interfacial charge-transfer processes occurring in the DSSC (**b**). Also shown is the blocking function of ZnO blocking layer on interfacial recombination as described in this paper.

the decreased electron transit time reveals that the suppression effect is stronger than the potential barrier effect when the ZnO layer thickness is smaller than 20 nm. The obtained values of L_n/d of cells IV to VII are shown in Table 2, which are all larger than that of the reference cell without ZnO layer, with the largest value of 8.4 for cell VI with a 15-nm-thick ZnO blocking layer. As a consequence, J_{sc}'s of the four cells are significantly improved and reaches the largest value of 17.3 mA cm^{-2} for cell VI. No matter significant improvement of J_{sc}'s for the four cells, little variation in V_{oc} is found for cells with and without ZnO layers, manifesting no electrons accumulate at the interface between ZnO and TiO_2, which is in good agreement with the rapid transport of injected electrons in TiO_2 conduction band to FTO substrates through ZnO layers.

Conclusions

In summary, thick electrospun TiO_2 nanofibers sintered at 500°C to 600°C were used as photoanodes to fabricate DSSCs. The remarkable electron diffusion length in TiO_2 nanofiber cells is the key point that makes it feasible to use thick photoanode to obtain high photocurrent and high conversion efficiency. Besides, at sintering temperature of 550°C, a small rutile content in the nanofiber (approximately 15.6%) improved conversion efficiency, short-circuit current, and open-circuit voltage of the cell by 10.9%, 7.4%, and 1.35%, respectively. Moreover, it is demonstrated that ultrathin ZnO layer prepared by ALD method could effectively suppress the electron transfer from FTO to electrolytes by IMVS measurements, and its suppression effect of back reaction was stronger than the potential barrier effect of electron transfer from TiO_2 to FTO by IMPS measurements. A large ratio of electron diffusion length to photoanode thickness (L_n/d) was obtained in the approximately 40-μm-thick TiO_2 nanofiber DSSC with a 15-nm-thick ZnO blocking layer, which is responsible for short-circuit current density of 17.3 mA cm^{-2} and conversion efficiency of 8.01%. The research provides a potential approach to fabricate high-efficient DSSCs.

Abbreviations

ALD: atomic layer deposition; DSSCs: dye-sensitized solar cells; FF: fill factor; FTO: fluorine-doped SnO_2; IMPS: intensity-modulated photocurrent spectroscopy; IMVS: intensity-modulated photovoltage spectroscopy; J_{sc}: short-circuit current; *J-V*: photocurrent-voltage; PCE: photoelectric conversion efficiency; PVP: polyvinylpyrrolidone; SEM: scanning electron microscope; V_{oc}: open-circuit voltage; XRD: X-ray diffraction; 1-D: one-dimensional; τ_d: transit time; τ_n: electron lifetime.

Competing interests

The authors declare that they have no competing interests.

Authors' contributions

JND and NYN conceived and designed the experiments, and wrote the paper. YL carried out the experiments and took part in writing. HH and LB participated in the experiments. SZ participated in the discussion and correction of the paper. All authors read and approved the final manuscript.

Acknowledgements

This work was supported by the National High Technology Research and Development Program 863 (2011AA050511), Jiangsu '333' Project, and the Priority Academic Program Development of Jiangsu Higher Education Institutions.

Received: 29 November 2012 Accepted: 27 December 2012
Published: 3 January 2013

References

1. Yella A, Lee HW, Tsao HN, Yi C, Chandiran AK, Nazeeruddin MK, Diau EWG, Yeh CY, Zakeeruddin SM, Grätzel M: **Porphyrin-sensitized solar cells with cobalt (II/III)-based redox electrolyte exceed 12% efficiency.** *Science* 2011, **334:**629–634.
2. Lagemaat JVD, Park NG, Frank AJ: **Influence of electrical potential distribution, charge transport, and recombination on the photopotential and photocurrent conversion efficiency of dye-sensitized nanocrystallineTiO_2 solar cells: a study by electrical impedance and optical modulation techniques.** *J Phys Chem B* 2000, **104:**2044–2052.
3. Zhu K, Neale NR, Miedaner A, Frank AJ: **Enhanced charge-collection efficiencies and light scattering in dye-sensitized solar cells using oriented TiO_2 nanotubes arrays.** *Nano Lett* 2007, **7:**69–74.
4. Kang SH, Choi SH, Kang MS, Kim JY, Kim HS, Hyeon T, Sung YE: **Nanorod-based dye-sensitized solar cells with improved charge collection efficiency.** *Adv Mater* 2008, **20:**54–58.
5. Limmer SJ, Cao GZ: **Sol–gel electrophoretic deposition for the growth of oxide nanorods.** *Adv Mater* 2003, **15:**427–431.
6. Miao Z, Xu DS, Ouyang JH, Guo GL, Zhao XS, Tang YQ: **Electrochemically induced sol–gel preparation of single-crystalline TiO_2 nanowires.** *Nano Lett* 2002, **2:**717–720.
7. Kasuga T, Hiramatsu M, Hoson A, Sekino T, Niihara K: **Titania nanotubes prepared by chemical processing.** *Adv Mater* 1999, **11:**1307–1311.
8. Chen Q, Zhou WZ, Du GH, Peng LM: **Trititanate nanotubes made via a single alkali treatment.** *Adv Mater* 2002, **14:**1208–1211.
9. Zwilling V, Darque-Ceretti E, Boutry-Forveille A, David D, Perrin MY, Aucouturier M: **Structure and physicochemistry of anodic oxide films on titanium and TA6V alloy.** *Surf Interface Anal* 1999, **27:**629–637.
10. Zhao JL, Wang XH, Sun TY, Li LT: **In situ templated synthesis of anatase single-crystal nanotube arrays.** *Nanotechnology* 2005, **16:**2450–2454.
11. Krishnamoorthy T, Thavasi V, Subodh GM, Ramakrishna S: **A first report on the fabrication of vertically aligned anatase TiO_2 nanowires by electrospinning: preferred architecture for nanostructured solar cells.** *Energ Environ Sci* 2011, **4:**2807–2812.
12. Lee BH, Song MY, Jang SY, Jo SM, Kwak SY, Kim DY: **Charge transport characteristics of high efficiency dye-sensitized solar cells based on electrospun TiO_2 nanorod photoelectrodes.** *J Phys Chem C* 2009, **113:**21453–21457.
13. Dong ZX, Kennedy SJ, Wu YQ: **Electrospinning materials for energy-related applications and devices.** *J Power Sources* 2011, **196:**4886–4904.
14. Song MY, Ahn YR, Jo SM, Kim DY, Ahn JP: **TiO_2 single-crystalline nanorod electrode for quasi-solid-state dye-sensitized solar cells.** *Appl Phys Lett* 2005, **87:**113113.
15. Kim ID, Rothschild A, Lee BH, Kim DY, Jo SM, Tuller HL: **Ultrasensitive chemiresistors based on electrospun TiO_2 nanofibers.** *Nano Lett* 2006, **6:**2009–2013.
16. Kokubo H, Ding B, Naka T, Tsuchihira H, Shiratori S: **Multi-core cable-like TiO_2 nanofibrous membranes for dye-sensitized solar cells.** *Nanotechnology* 2007, **18:**165604–6.
17. Mohamed AE, Rohani S: **Modified TiO_2 nanotube arrays (TNTAs): progressive strategies towards visible light responsive photoanode, a review.** *Energ Environ Sci* 2011, **4:**1065–1086.
18. Shankar K, Mor GK, Prakasam HE, Yoriya S, Paulose M, Varghese OK, Grimes CA: **Highly-ordered TiO_2 nanotube arrays up to 220 μm in length: use in water photoelectrolysis and dye-sensitized solar cells.** *Nanotechnology* 2007, **18:**1–11.
19. Li GH, Richter CP, Milot RL, Cai L, Schmuttenmaer CA, Crabtree RH, Brudvig GW, Batista VS: **Synergistic effect between anatase and rutile TiO_2 nanoparticles in dye-sensitized solar cells.** *Dalton Trans* 2009, **45:**10078–10085.
20. Yun TK, Park SS, Kim D, Shim JH, Bae JY, Huh S, Won YS: **Effect of the rutile content on the photovoltaic performance of the dye-sensitized solar cells composed of mixed-phase TiO_2 photoelectrodes.** *Dalton Trans* 2012, **41:**1284–1288.
21. Cameron PJ, Peter LM: **Characterization of titanium dioxide blocking layers in dye-sensitized nanocrystalline solar cells.** *J Phys Chem B* 2003, **107:**14394–14400.
22. Yu H, Zhang SQ, Zhao HJ, Will G, Liu PR: **An efficient and low-cost TiO_2 compact layer for performance improvement of dye-sensitized solar cells.** *Electrochim Acta* 2009, **54:**1319–1324.
23. Hattori R, Goto H: **Carrier leakage blocking effect of high temperature sputtered TiO_2 film on dye-sensitized mesoporous photoelectrode.** *Thin Solid Films* 2007, **515:**8045–8049.
24. Ahn KS, Kang MS, Lee JW, Kang YS: **Effects of a surfactant-templated nanoporous TiO_2 interlayer on dye-sensitized solar cells.** *J ApplPhys* 2007, **101:**084312.
25. Peng B, Jungmann G, Jager C, Haarer D, Schmidt HW, Thelakkat M: **Systematic investigation of the role of compact TiO_2 layer in solid state dye-sensitized TiO_2 solar cells.** *Coordin Chem Rev* 2004, **248:**1479–1489.
26. Xia J, Masaki N, Jiang K, Yanagida S: **Sputtered Nb_2O_5 as a novel blocking layer at conducting glass/TiO_2 interfaces in dye-sensitized ionic liquid solar cells.** *J PhysChem C* 2007, **111:**8092–8097.
27. Perez-Hernandez G, Vega-Poot A, Perez-Juarez I, Camacho JM, Ares O, Rejon V, Pena JL, Oskam G: **Effect of a compact ZnO interlayer on the performance of ZnO-based dye-sensitized solar cells.** *Sol Energ Mat Sol C* 2012, **100:**21–26.
28. Liu YM, Sun XH, Tai QD, Hu H, Chen BL, Huang N, Sebo B, Zhao XZ: **Influences on photovoltage performance by interfacial modification of FTO/mesoporous TiO_2 using ZnO and TiO_2 as the compact film.** *J Alloy Compd* 2011, **509:**9264–9270.
29. Zhang HZ, Banfield JF: **Understanding polymorphic phase transformation behavior during growth of nanocrystalline aggregates: insights from TiO_2.** *J Phys Chem B* 2000, **104:**3481–3487.
30. Kruger J, Plass R, Gratzel M, Cameron PJ, Peter LM: **Charge transport and back reaction in solid-state dye-sensitized solar cells: a study using intensity-modulated photovoltage and photocurrent spectroscopy.** *J Phys Chem B* 2003, **107:**7536–7539.
31. Bandic ZZ, Bridger PM, Piquette EC, McGill TC: **Electron diffusion length and lifetime in p-type GaN.** *Appl Phys Lett* 1998, **73:**3276.
32. Wang M, Chen P, Humphry-Baker R, Zakeeruddin SM, Gratzel M: **The influence of charge transport and recombination on the performance of dye-sensitized solar cells.** *Chemphyschem* 2009, **10:**290–299.
33. Gregg BA, Hanna MC: **Comparing organic to inorganic photovoltaic cells: theory, experiment, and simulation.** *J Appl Phys* 2003, **93:**3605–3614.

doi:10.1186/1556-276X-8-9
Cite this article as: Ding *et al.*: The influence of anatase-rutile mixed phase and ZnO blocking layer on dye-sensitized solar cells based on TiO_2nanofiberphotoanodes. *Nanoscale Research Letters* 2013 **8**:9.